

AN INTEGRATED ANALYSIS FOR THE PASSING SHIP PROBLEM ON SANTOS PORT CONSIDERING REAL-TIME SIMULATIONS AND MOORED SHIP DYNAMICS

by

R. A. Watai¹, F. Ruggeri¹, E. A. Tannuri² and K. Nishimoto²

ABSTRACT

An integrated analysis methodology for the passing ship problem considering real-time simulations and moored ship dynamics is presented. The methodology is introduced as an alternative to the traditional method, which defines a criterion based only on safe distances and maximum velocities, neglecting crucial navigation aspects of the ship. In this sense, the proposed methodology extends the standard one by including results of pilot guided real-time simulations into the analysis process. An application of the method analyzing the effects caused by the passage of a 366 m long container ship next to small capsized vessels moored at different berths of the Port of Santos, Brazil, is presented. Results are discussed by means of moored ship motions and mooring loads, including also possible improvements on the mooring arrangements applied nowadays in the port.

1. INTRODUCTION

The search of the shipping line companies to achieve economies of scale has given rise to sharply growths of container ship sizes in the last years, increasing the port challenges to improve its capabilities. Besides the necessity of physical interventions on the access channel depth and turning basins, redefinition of tug bollard pull requirements, among others, the port new facilities must also be prepared to provide safe mooring conditions to the moored ships that will be subjected to strong hydrodynamic interaction effects induced by the passing of the new large vessels. This interaction effect, for instance, can result in the rupture of the mooring lines, emergency unberthing as well as damages to the loading and offloading pieces of equipment, being the main cause of some accidents occurred in the past, such as, the ones involving the ships New York and Titanic, when leaving Southampton, in April 1912, and ships Buffalo and Jupiter in September 1990.

(Remery, 1974), one of the first authors to study the passing ship problem, has conducted an experimental campaign for measuring the forces on captive and moored tanker vessels under the passage of another tanker ship, investigating the influence of passing ship size, distance to the moored ship, loading conditions, speed, as well as the effects of mooring system stiffness. (Flory, 2002) has applied Remery's experimental data to propose a set of equations to calculate peak forces and moments produced by the passing tanker ships, in which corrections to other under keel clearance (UKC) were also proposed based on data given in (Muga & Feng, 1975). Other examples of extensive model test programs and empirical formulas for the loads involved in the passing ship problem are presented in (Vantorre, Verzhbitskaya, & Laforce, 2002) and (Kriebel, 2005).

With the increasing of computational capacity, numerical models capable of simulating the time-dependent fluid flow and pressure field of the passing ship problem are being often more applied. Over the last years, 3D panel methods based on the potential flow theory have been the most often applied technique to model the passing ship problem. (Korsmeyer, Lee, & Newman, 1993) are one of the first to apply a double-body potential model to the analysis of ship interactions, in which, at moderate Froude number, the interaction loads were calculated by neglecting free surface effects and shed vorticity. (Pinkster J. , 2004) has investigated the passing ship problem including free surface effects by developing a method based on the mixed application of the double-body model and linear wave diffraction computations, from where he has verified significant free surface effects in a situation where the ship is moored in a confined dock positioned next to a canal where the passing ship sails and very low contributions of the free surface effects for passing ships sailing next to vessels moored at open waters or along vertical quay walls. Again, the results were generated at moderate Froude number.

More recently, several investigations focusing on the passing ship problem were performed in the context of the Joint Industry Project ROPES ("Research on Passing Ship Effects on Ships"), which culminated in the development of the user-friendly software tool ROPES (see (Pinkster J. A., 2014)). For such development, full-scale field measurements (Wictor & van den Boom, 2014) and scaled model tests (see (Talstra & Bliet, 2014) and (van der Hout & de Jong, 2014)) have been carried out

¹ Argonáutica Engineering & Research, watai@argonautica.com.br

² University of São Paulo, Numerical Offshore Tank, Brazil

for validation purposes, what enabled one to determined the limitations and versatility of the ROPES software under many different geometries (e.g. straight channel and complex harbour configurations) and current conditions (e.g. following and counter currents). Moreover, (Talstra & Bliet, 2014) have also proposed a correction factor which compensates the ROPES underprediction in high-Froude number range (> 0.3), which was mainly attributed to the fact the free-surface effects are not included in the double-body model.

The present paper presents a methodology to support the definition of operational limits to passing ships based on the use of a in-house potential flow solver for the calculation of the hydrodynamic interaction forces, a dynamic simulator to evaluate the passing ship impacts on the moored ship motions and mooring system loads, and also real-time simulations campaigns that provides maneuverings paths of the passing ship along port navigation channels. Differently from the common approach of defining operational limits based exclusively on safe minimum distances and maximum allowable speeds extracted by parallel passing ship analysis, in this approach pilot oriented ship trajectories and velocities are incorporated into the analysis. This is indeed an important aspect to be included in the definition of operational limits because in many circumstances it is not possible to restrict the ship forward speed to the maximum velocity established by the passing ship analysis, either for keeping the ship rudder efficiency or by the simple fact that even the ship dead slow speed is higher than the safe limit value.

The proposed methodology starts with the definition of the berths most susceptible to the passing ship problem, as well as the selection of typical ships. Approximate ship maneuvering trajectories with different distances to the berths are then prescribed and used for the calculations of the interaction forces time histories, mooring loads and ship motions, these being compared to operational limits criteria, providing a first estimate of safe speed and distance to moored ships. At this stage, inbound and outbound real-time maneuvering simulations are conducted by local pilots with the aid of colored areas (defined by passing speed and distance to moored ships) printed in the electronic nautical chart highlighting the main risk zones. Further ahead, the hydrodynamic interactions forces and mooring system loads are recalculated with the updated ship trajectories, which were resulted from the pilot's instructions during the real-time simulations. Finally, recommendations are provided in terms of the new ship maneuvering and improvements (if applicable) on the mooring system arrangements.

In order to illustrate the procedure, the methodology is applied to analyze the maneuvering feasibility of a 366 m long contained ship in the curve and narrow channel of the Port of Santos, Brazil. With such purpose, it is considered the use of a dynamic simulator of moored ships berthed alongside quay walls (MeDuSa[®]), the real-time simulator of the Numerical Offshore Tank of the University of São Paulo (Tannuri, et al., 2014) and a derivative version of the program TDRPM (Time Domain Rankine Panel Method), a 3D-BEM originally developed for solving seakeeping problems of floating systems (see (Watai, 2015) and (Watai, Ruggeri, Sampaio, & Simos, 2015)), which was adapted to applications on the passing ship problem as previously presented in (Watai, Ruggeri, Tannuri, & Weiss, 2013) and (Ruggeri, Watai, & Tannuri, 2016). The description of the numerical models applied is presented next.

2. NUMERICAL MODELS

2.1. Mooring Design System (MeDuSa[®]) Tool

In MeDuSa[®], the ship motions are formulated in time domain under the retardation function approach for the hydrodynamic reaction forces, as proposed in (Cummins, 1962). This is a usual approach when considering arbitrary time varying excitation forces, not restricting, therefore, the formulation to steady state oscillatory motions with frequency independent hydrodynamic coefficients. As already discussed in (Oortmerssen, 1976), the assumption of constant hydrodynamic coefficients cannot be justified, especially in shallow water and near quay walls where these coefficients appear to be very sensitive to changes in frequency.

$$(\mathbf{M} + \mathbf{A}(\omega_\infty))\ddot{\mathbf{x}}(t) + \int_0^\infty \mathbf{R}(\tau)\dot{\mathbf{x}}(t - \tau)d\tau + \mathbf{K}\mathbf{x}(t) = \mathbf{f}_{ext}(t) + \mathbf{f}_{ext}^{visc}(t) \quad (1)$$

In (1), \mathbf{M} denotes body mass/inertia matrix, $\mathbf{A}(\omega_\infty)$ the added mass/inertia matrix at infinite frequency, $\mathbf{R}(\tau)$ is the retardation functions matrix, \mathbf{x} the ship motions vector for the six degrees of freedom (surge, sway, heave, roll, pitch and yaw), \mathbf{K} is the linear hydrostatic restoring coefficient matrix, $\mathbf{f}_{ext}(t)$ is external forces and moments vector, which are composed by forces due to current, wind, passing ships and mooring systems, and $\mathbf{f}_{ext}^{visc}(t)$ is external damping forces and moments of viscous origin.

The hydrodynamic coefficients $\mathbf{A}(\omega_\infty)$ and $\mathbf{R}(\tau)$ are calculated externally by solving the so-called radiation problem in frequency domain using a higher order BEM code based on the linearized free

surface Green's function. The damping forces $f_{ext}^{visc}(t)$ are considered by splitting it in linear (B^{lin}) and quadratic terms (B^{quad}), as presented in (2).

$$f_{ext}^{visc}(t) = -B^{lin}x(t) - x^T(t)B^{quad}x(t) \quad (2)$$

These coefficients stand for the viscous linear roll damping, as well as fluid reactive forces on the moored ship in surge, sway and yaw mode, defined following (OCIMF, 2008) convention:

$$B_{11}^{quad} = \frac{1}{2}\rho C_{c,1}L_{pp}T \quad B_{22}^{quad} = \frac{1}{2}\rho C_{c,2}L_{pp}T \quad B_{66}^{quad} = \frac{1}{2}\rho C_{c,6}L_{pp}^2T \quad (3)$$

where T and L_{pp} are the ship draft and length between perpendiculars, respectively, and $C_{c,j}$ are the current drag coefficients for the j degree of freedom (here, only surge, sway and yaw motions are considered).

The mooring lines and fenders are represented by nonlinear spring elements and characterized by their respective undeformed lengths l_i and d_i , nonlinear load-elongation curves f_i^l , nonlinear reaction deflection curves f_i^f , initial coordinates of the ship chocks $(x_{i,0}^c, y_{i,0}^c, z_{i,0}^c)$ and the positions of the bollards (x_i^b, y_i^b, z_i^b) and fenders along the quay (x_i^f, y_i^f, z_i^f) . The simulation starts with the center of gravity of the moored ship at the origin of the fixed coordinate system and with the i_{th} line set with an user defined amount of pretension $L_{i,0}$ that results in initials line lengths $l_{i,0}$ and elongations $\delta l_{i,0} = l_{i,0} - l_i$. Figure 1 shows a schematic representation of the coordinate system and the main mooring system elements considered by MeDuSa[®].

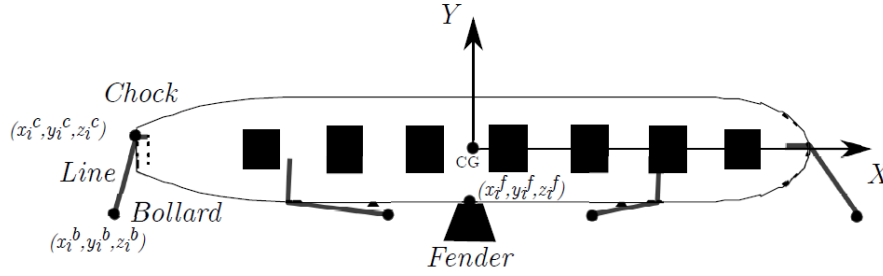


Figure 1: Definition of coordinate system and mooring system elements

Assuming small rotative motions, the instantaneous coordinates of the ship chocks can be written in terms of the six degrees of freedom ship rigid modes (x_1, x_2, \dots, x_6) , as presented in (4).

$$\begin{aligned} x_i^c(t) &= x_{i,0}^c + x_1(t) - x_6(t)y_{i,0}^c + x_5(t)z_{i,0}^c \\ y_i^c(t) &= y_{i,0}^c + x_6(t)x_{i,0}^c + x_2(t) - x_4(t)z_{i,0}^c \\ z_i^c(t) &= z_{i,0}^c - x_5(t)x_{i,0}^c + x_5(t)y_{i,0}^c + x_3(t) \end{aligned} \quad (4)$$

The mooring line loads $L_i(t)$ are determined through the nonlinear load-elongation curves $f_i^l(\varepsilon_i^l(t))$, i.e.

$$\begin{aligned} L_i(t) &= f_i^l(\varepsilon_i^l(t)) \quad \text{if } \Delta l_i(t) > 0 \quad (\text{tensioned}) \\ L_i(t) &= 0 \quad \text{if } \Delta l_i(t) \leq 0 \quad (\text{slack}) \end{aligned} \quad (5)$$

where $\Delta l_i(t)$ and $\varepsilon_i^l(t)$ are the instantaneous line deformation and elongation, respectively, which are defined in terms of the instantaneous line length $l_{i,f}(t)$, as follows:

$$\begin{aligned} l_{i,f}(t) &= \sqrt{(x_i^c(t) - x_i^b)^2 + (y_i^c(t) - y_i^b)^2 + (z_i^c(t) - z_i^b)^2} \\ \Delta l_i(t) &= l_{i,f}(t) - l_{i,0} + \delta l_{i,0} = l_{i,f}(t) - l_i \\ \varepsilon_i^l(t) &= \Delta l_i(t)/l_i \end{aligned} \quad (6)$$

The resulting forces and moment about the ship center of gravity induced by the N_l mooring line are calculated following (7).

$$\begin{aligned}
 f_{ext,1}^l(t) &= \sum_{i=1}^{N_l} L_i(t) (x_i^b - x_i^c(t)) / l_{i,f}(t) \\
 f_{ext,2}^l(t) &= \sum_{i=1}^{N_l} L_i(t) (y_i^b - y_i^c(t)) / l_{i,f}(t) \\
 f_{ext,3}^l(t) &= \sum_{i=1}^{N_l} L_i(t) (z_i^b - z_i^c(t)) / l_{i,f}(t) \\
 f_{ext,4}^l(t) &= \sum_{i=1}^{N_l} -f_{ext,2}^l(t)(z_i^c(t) - x_3(t)) + f_{ext,3}^l(t)(y_i^c(t) - x_2(t)) \\
 f_{ext,5}^l(t) &= \sum_{i=1}^{N_l} f_{ext,1}^l(t)(z_i^c(t) - x_3(t)) - f_{ext,3}^l(t)(x_i^c(t) - x_1(t)) \\
 f_{ext,6}^l(t) &= \sum_{i=1}^{N_l} -f_{ext,1}^l(t)(y_i^c(t) - x_2(t)) + f_{ext,2}^l(t)(x_i^c(t) - x_1(t))
 \end{aligned} \tag{7}$$

The fenders loads are split in reaction $D_i^r(t)$ and friction forces $D_i^f(t)$, in which the former is calculated through the nonlinear deformation-reaction curves $f_i^f(-d_i(t))$, described in (8), and acts on the ship only in the transversal direction Y , whereas the friction force is calculated through Coulomb's expression (9) and acts on the body exclusively in the longitudinal direction X . In these equations, μ is the fender friction coefficient and the fender deformation $d_i(t)$ is found by (10).

$$\begin{aligned}
 D_i^r(t) &= f_i^f(-d_i(t)) \quad \text{if } d_i(t) < 0 \quad (\text{compressed}) \\
 D_i^r(t) &= 0 \quad \text{if } d_i(t) \geq 0 \quad (\text{not in contact})
 \end{aligned} \tag{8}$$

$$\begin{aligned}
 D_i^f(t) &= -\text{sgn}(\dot{x}_1)\mu D_i^r(t) \quad \text{if } d_i(t) < 0 \quad (\text{compressed}) \\
 D_i^f(t) &= 0 \quad \text{if } d_i(t) \geq 0 \quad (\text{not in contact})
 \end{aligned} \tag{9}$$

$$d_i(t) = x_2(t) + (x_i^f - x_1(t))x_6(t) - (z_i^f - x_3(t))x_4(t) \tag{10}$$

Finally, resulting forces and moments about the ship center of gravity of the N_f fenders are determined by expressions in (11).

$$\begin{aligned}
 f_{ext,1}^f(t) &= \sum_{i=1}^{N_f} D_i^f(t) \quad f_{ext,2}^f(t) = \sum_{i=1}^{N_f} D_i^r(t) \quad f_{ext,3}^f(t) = 0 \\
 f_{ext,4}^f(t) &= \sum_{i=1}^{N_f} -f_{ext,2}^f(t)(z_i^f - x_3(t)) \quad f_{ext,5}^f(t) = 0 \\
 f_{ext,6}^f(t) &= \sum_{i=1}^{N_f} f_{ext,2}^f(t)(x_i^f - x_1(t))
 \end{aligned} \tag{11}$$

The external forces $f_{ext}^l(t)$ and $f_{ext}^f(t)$ are then combined to the others on the right hand-side of (1), which is solved numerically by a Runge Kutta 4th order method. As output of the computations, MeDuSa[®] provides the time histories of ship motions, mooring lines and fender loads.

2.2. Hydrodynamic Interaction Forces

The external force and moments induced by the passing ship on the moored vessel are calculated by a 3D panel method upon the considerations of potential flow theory, in which the velocity field is defined by the gradient of the velocity potential $\Phi(\mathbf{X})$, where \mathbf{X} is a vector in the earth-fixed reference frame (X, Y, Z) that is defined such that X and Y axes lie on the plane of the free surface and Z axis points upwards and out of the fluid volume. In addition, for each independent body, right-hand oriented body-fixed reference frames $\mathbf{x} = (x, y, z)$, centered at the center of gravity of the bodies, are used to describe the body geometries and resultant forces and moments, in which x and y axes point to ship's bow and port side, respectively.

The double-body formulation here applied assumes the passing ship sailing at moderate Froude number and neglects the free surface effects and shed vorticity. The governing equations for determining $\Phi(\mathbf{X})$ are defined by Laplace's equation:

$$\nabla^2\phi = 0 \text{ in fluid domain} \quad (12)$$

under the following boundary conditions (BC):

$$\nabla\phi \cdot \mathbf{n}_{fs} = 0 \text{ on } S_{fs} \text{ (Free Surface rigid-lid BC)} \quad (13)$$

$$\nabla\phi \cdot \mathbf{n}_m = 0 \text{ on } S_m \text{ (Moored vessel no-flux BC)} \quad (14)$$

$$\nabla\phi \cdot \mathbf{n}_p = U(t) \cdot \mathbf{n}_p \text{ on } S_p(t) \text{ (Passing Ship no-flux BC)} \quad (15)$$

$$\nabla\phi \cdot \mathbf{n}_{fix} = 0 \text{ on } S_{fix} \text{ (Bottom and port structures no-flux BC)} \quad (16)$$

$$\nabla\phi \rightarrow 0 \text{ at } \sqrt{X^2 + Y^2 + Z^2} \rightarrow \infty \text{ (Far field evanescent condition)} \quad (17)$$

where \mathbf{n} and S are the normal unit vector with positive direction into the fluid and the wetted surfaces of the bodies and other port structure surfaces. Besides that, the subscripts fs , m , p and fix refer to the free surface, moored ship, passing ship and all fixed surfaces (bottom, quay wall, banks etc.), respectively.

A similar numerical scheme presented in (Hess & Smith, 1967) has been applied to solve the boundary value problem by introducing a distribution of Rankine's sources with density σ on all wetted surfaces:

$$\phi(\mathbf{P}) = \iint_{\partial\Omega} \sigma(\mathbf{Q})G(\mathbf{P}, \mathbf{Q})d\partial\Omega(\mathbf{Q}) \quad (18)$$

where $\mathbf{P}(x_p, y_p, z_p)$ and $\mathbf{Q}(x_q, y_q, z_q)$ are the respective field and the source points on all wetted surfaces S , and $G(\mathbf{P}, \mathbf{Q})$ is the Green's function constructed to satisfy the free surface rigid-lid, bottom (at $Z = -h$) and fair field boundary conditions:

$$G(\mathbf{P}, \mathbf{Q}) = \sum_{i=-\infty}^{\infty} \left(\frac{1}{r_i} + \frac{1}{r'_i} \right) \quad (19)$$

where:

$$r_i = \sqrt{(x_p - x_q)^2 + (y_p - y_q)^2 + (z_p + z_q + 2ih)^2} \quad (20)$$

$$r'_i = \sqrt{(x_p - x_q)^2 + (y_p - y_q)^2 + (z_p - z_q + 2ih)^2} \quad (21)$$

The boundary conditions on wetted surfaces are then imposed by the following integral equation:

$$2\pi\sigma(\mathbf{P}) = \iint_{\partial\Omega} \sigma(\mathbf{Q}) \frac{\partial G(\mathbf{P}, \mathbf{Q})}{\partial n(\mathbf{P})} d\partial\Omega(\mathbf{Q}) = f(\mathbf{P}) \quad (22)$$

in which the right-hand side term $f(\mathbf{P})$ reads $f(\mathbf{P}) = \mathbf{U}(\mathbf{P}) \cdot \mathbf{n}(\mathbf{P})$ for the boundary condition of the passing ship and $f(\mathbf{P}) = 0$ for the other surfaces.

Once (22) is solved for an specific position of the sailing ship, the components of the force and moment acting on the moored ship are calculated by integrating the pressure from Bernoulli's equation over the body surface, as expressed in (23) and (24), where A_j is the area of the j -panel.

$$\mathbf{F} = -\rho \sum_{j=1}^N \left(\frac{\partial\phi_j}{\partial t} + \frac{1}{2} \nabla\phi_j \phi_j \right) \mathbf{n}_j A_j \quad (23)$$

$$\mathbf{M} = -\rho \sum_{j=1}^N \left(\frac{\partial\phi_j}{\partial t} + \frac{1}{2} \nabla\phi_j \phi_j \right) (\mathbf{r}_j \times \mathbf{n}_j) A_j \quad (24)$$

2.3. Real-Time Maneuvering Simulator

The real-time simulator of the Numerical Offshore Tank of the University of São Paulo (TPN-USP) was applied for conducting the maneuvering simulations with the container ship of length 366m. This simulator was officially opened in 2012 and is a result of several research projects that have been conducted during more than ten years in close cooperation with Petrobras, research institutes and universities. It consists on a Full Mission Maneuvering Simulator with 270° field view comprised by a 12m diameter screen, 30 image projectors, 10 panels for commands and instruments, and 4 overhead screens, immersing the pilots and ship masters into very realistic scenarios. The description of the numerical model adopted is presented in (Tannuri, et al., 2014). The Figure 2 shows the pilot in the simulator bridge during the 366m long container ship simulation.



Figure 2: Pilot in the real-time simulator bridge

3. APPLICATION TO THE PORT OF SANTOS

3.1. Selection of critical berths and ships

As a first step of the methodology, twelve berths have been selected by the local port authority (CODESP) and pilots as the most critical berths of the port in terms of the passing ship problem. The locations of the berths along the channel are presented in Figure 3. For the sake of conciseness and to focus on the understanding of the analysis methodology, only the berth 21, which presented the largest number of fail cases in the real-time simulations, will be considered. The berth 21 is equipped with T-Head bollards of capacity 100 tf and π -type fenders (MV1000L1500) of maximum energy absorption and reaction of 71.4 tfm and 155.4 tf, respectively. The water depth considered in the analysis was 16 m.

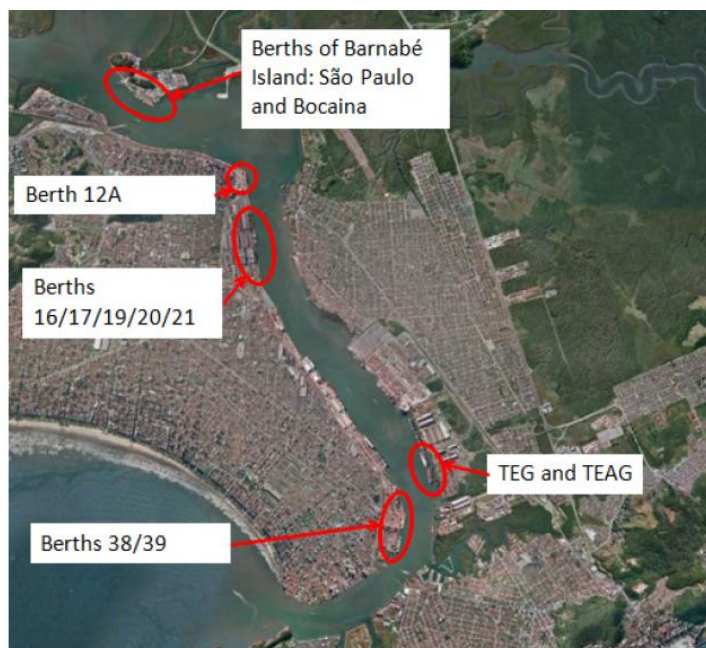


Figure 3: Critical berths in terms of passing ships problem in Port of Santos

The moored vessel selected to be analyzed is a Small Capesize ship of 125,000 tons of deadweight, 275m long, 43 m width, 22.4 m height and draft 14.2 m. This ship is normally equipped with 12 polyblend lines of diameter 72 mm and Minimum Breaking Load (MBL) of 84 tf. The lines Load x Elongation and fenders nonlinear Reaction x Deflection curves are presented in Figure 4.

Typical mooring arrangement applied in the Port of Santos has been applied, being composed of 12 mooring lines spread in 4 stern lines, 2 stern springs, 2 bow springs and 4 head lines. In an equilibrium position, the ship side hull touches 10 fenders. The mooring arrangement is shown in Figure 5.

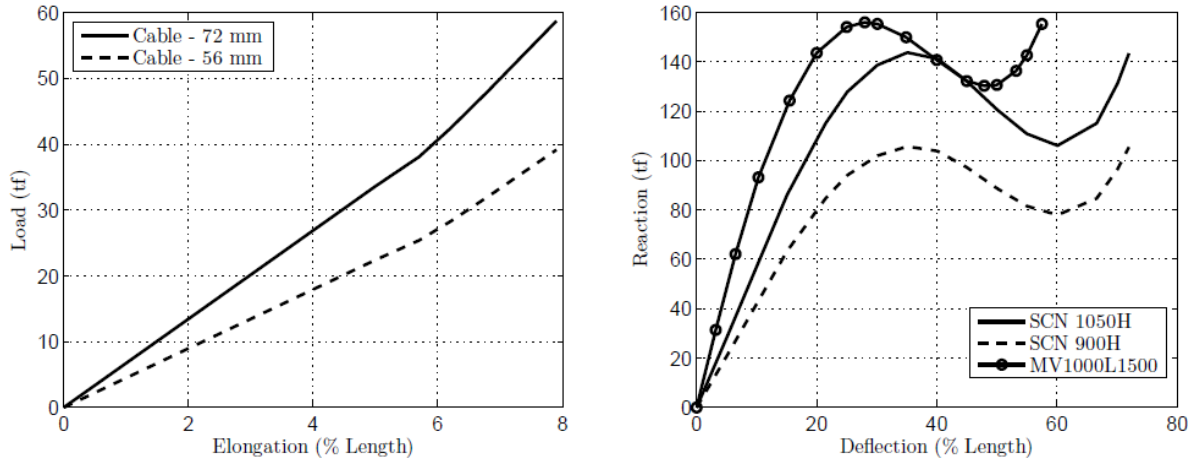


Figure 4: Line Load x Elongation (left) and Fender Reaction x Deflection curves (right).
Sources: (OCIMF, 2008) and (Trelleborg, 2017)

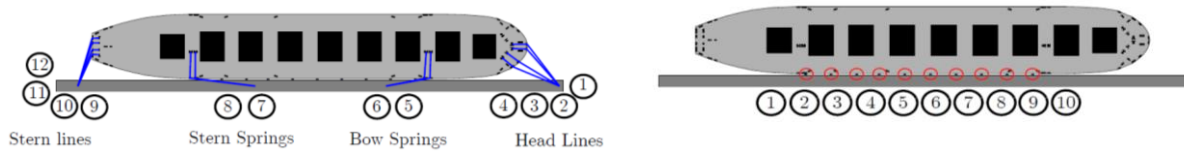


Figure 5: Mooring arrangement of small capsized at berth 21. Mooring lines (left) and fenders (right)

3.2. Preliminary Hydrodynamic Interaction Loads and Mooring Calculations

As aforementioned, the passing effects are analyzed considering the maneuvering of a 366 m long container ship, whose main dimensions and gear features are presented in Table 1.

Table 1: Main characteristics of the sailing ship

Cargo capacity	13,8	[TEU]
Deadweight	124,479	[ton]
Ship Length (LOA)	366	[m]
Ship Beam	51.2	[m]
Ship Draft	14.2	[m]
Ship Height	29.9	[m]
Dead slow ahead	7.9	[m]
Slow ahead	10.8	[kts]
Half ahead	13.2	[kts]
Full speed	16	[kts]
Full sea speed	23.9	[kts]

The second step of the methodology is then dedicated to obtain first estimates of the passing ship safe speed and distance to the moored ship by analyzing the mooring loads and ship motions induced by the ship advancing on the prescribed trajectories illustrated in Figure 6, which correspond to minimum distances of 60m (on the right margin), 150m (on the center) and 230m (on the left margin) to the moored ship. For each prescribed trajectory, different sailing velocities in the range between 5kts and 10kts are also assumed.

The checking of failure cases is performed comparing the moored ship motions, line loads and fender compression forces with the safe working values recommended in (PIANC, 1995) and (OCIMF, 2008), here summarized in Table 2.

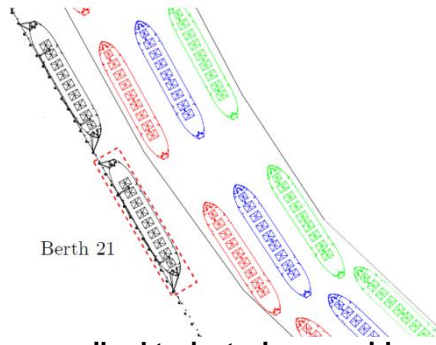


Figure 6: Ship maneuvering prescribed trajectories considered for the passing ship loads estimate at berth 21.

Table 2: Safe working values considered in the analysis

	Criteria	
Surge [m]	5.0	Peak-peak value
Sway [m]	2.5	Zero-peak value
Yaw [°]	3.0	Peak-peak value
Cables [tf]	42	50% of the line MBL
Fenders [tf]	105	100% of the fender maximum reaction

Figure 7 presents examples of moored ship hydrodynamic loads and motions induced by the container ship sailing at 7 kts under the different trajectories, whereas Figure 8 presents the loads on the mooring lines and fenders. Although, in this case, the small capesize motions did not exceed the criteria in any of the tested cases, there were some mooring lines and fenders that had their limits overtaken when the container ship passed by under the closest trajectory simulated.

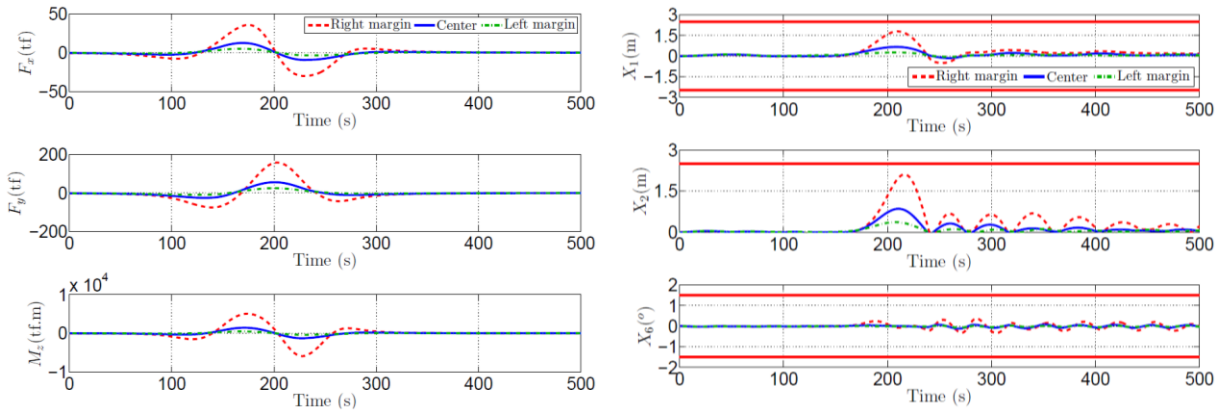


Figure 7: Moored ship hydrodynamic loads (left) and motions (right) time series induced by the container ship sailing at 7 kts. Solid horizontal lines indicate tolerated margins

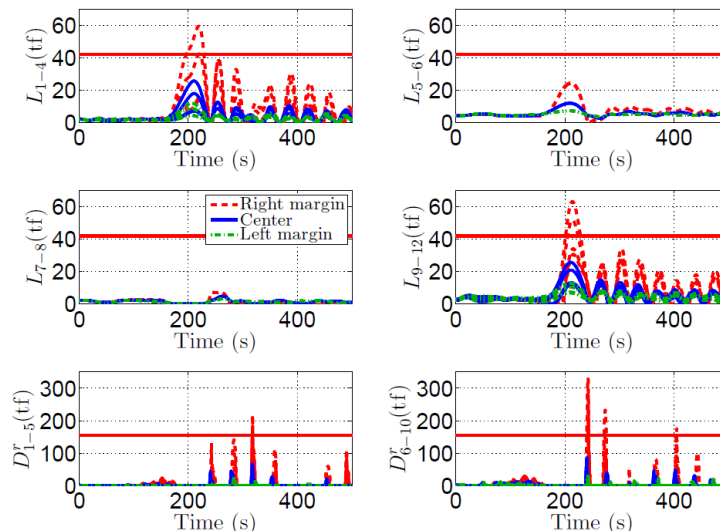


Figure 8: Moored ship mooring lines and fenders loads time series induced by the container ship sailing at 7 kts. Solid horizontal lines indicate tolerated margins

The results were made available as a guide for the pilots during the real-time simulations through operational maps which were also printed in the local nautical chart, as shown in Figure 9. The colored area in the nautical chart represents the conditions of passing distance and associated velocity, which the pilots should avoid crossing during the maneuvering in order to keep the mooring loads and motions of the moored vessel below the acceptable limits.

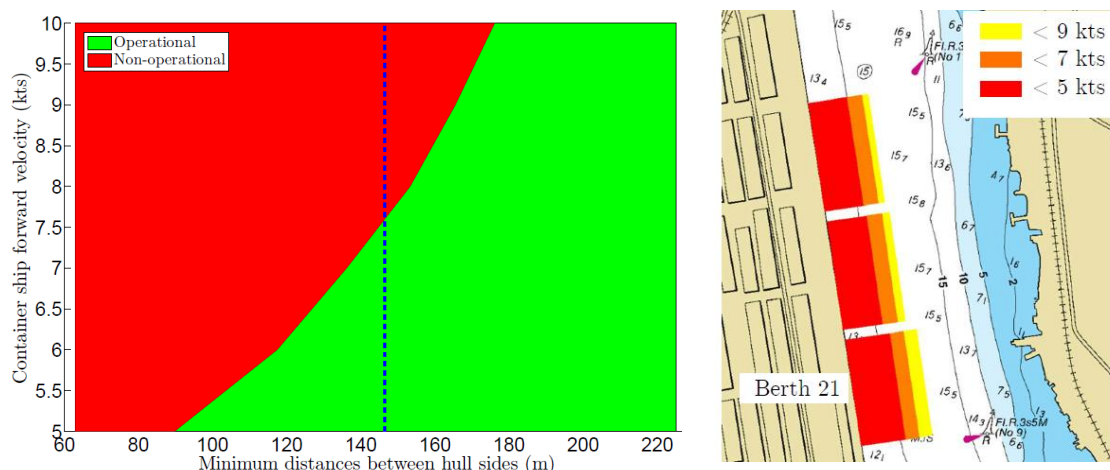


Figure 9: Operational limits in terms of passing distance and forward velocity for berth 21

3.3. Real Time Maneuvering Simulations

The proposed methodology now follows to the conduction of real-time simulations commanded by local and experienced pilots of the Port of Santos. This is a very important step of the present work, since it becomes possible to evaluate whether the ship can be indeed controlled and kept distant enough to the moored ships with relatively low speed. In total, 10 maneuvering simulations were carried out, comprising combinations of draft, outbound/inbound maneuvers, flood/ebb tides, wind and wave conditions, the latter acting only on the approach channel which is exposed to waves. Since the work methodology is here represented by the analysis of berth 21, the ship maneuvers that did not pass by this berth have been disregarded. Table 3 presents the simulation matrix with the main characteristics of each test, whereas Figure 10 presents some illustrative screenshots of the real-time simulation for Case 6, at different instants.

Table 3: Matrix of real-time maneuvering simulations

Case	Maneuvering	Current	Wind
1	Inbond	0.5 kts (ebb)	17 kts (E)
2	Outbound	0.5 kts (flood)	17 kts (E)
3	Inbond	0.8 kts (flood)	17 kts (E)
4	Outbound	0.8 kts (ebb)	17 kts (NW)
5	Inbond	0.8 kts (ebb)	17 kts (SW)
6	Inbond	0.8 kts (flood)	17 kts (NW)

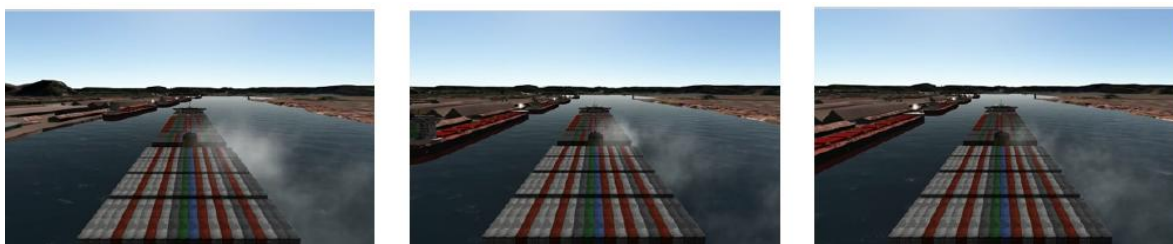


Figure 10: Screenshots of the real-time simulation at different instants during the passage of the container ship by the small capsize at berth 21, on the left

Figure 11 illustrates the forward velocity of the container ship when passing by berth 21. The two most critical cases are 4 and 6 in which neither the velocity nor the minimum recommended distance from berth 21 could be respected. As illustrated in Figure 11, the container ship has crossed the colored areas with forward velocities above 10 knots, exposing the small capsize mooring system to severe hydrodynamic interaction forces as will be presented ahead.

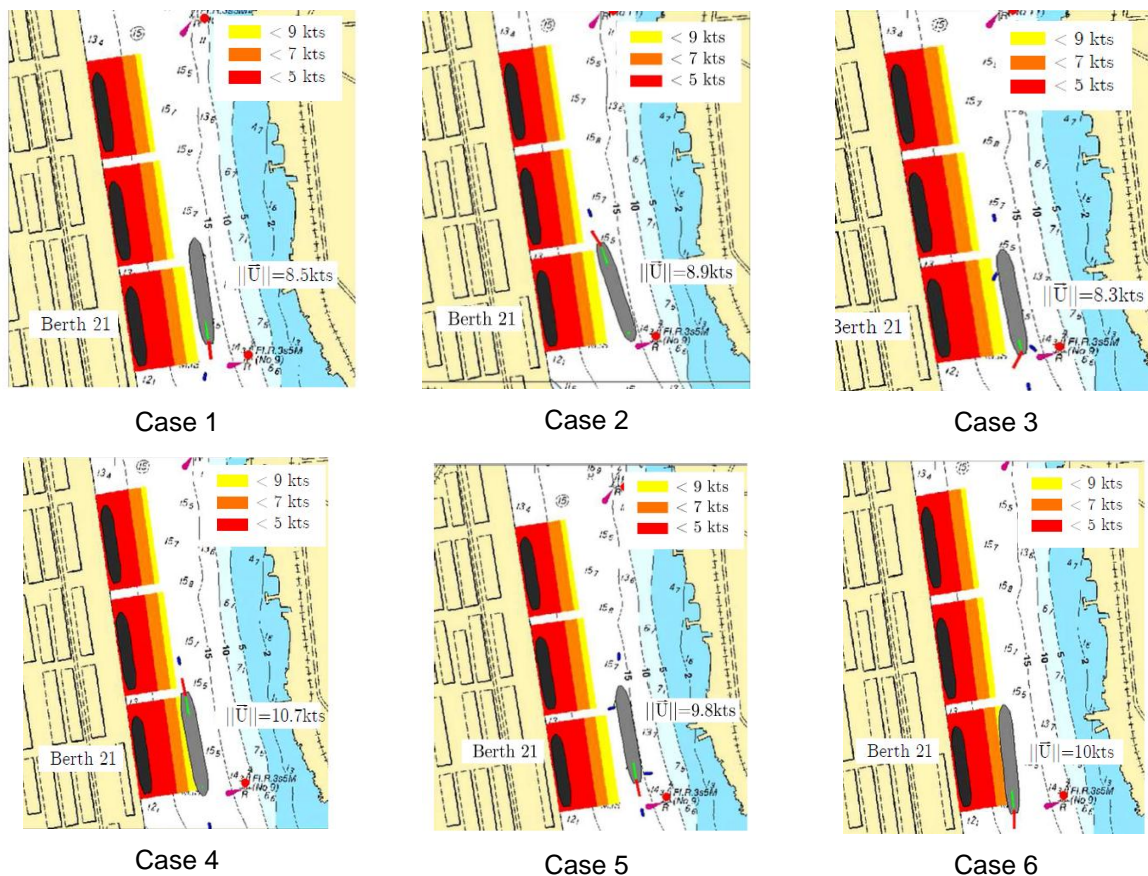


Figure 11: Container ship velocity when passing by berth for the 6 different cases

3.4. Reassessment of Ship Motions and Mooring Loads

In this stage of the methodology, the container ship trajectories and velocities obtained in the real-time simulations are used as input to calculate the ship motions and mooring loads by following the procedures aforementioned. For these simulations, the lines were set with low pre-tensions values of 2.2 tf (or 2.6% of MBL) in order to increase the conservatism of the analyses.

The obtained time histories of motions, mooring line loads and fender compression forces for the two most critical cases 4 and 6 are presented in Figure 12 and Figure 13, respectively. In addition, in case any of the criteria is exceeded, the correspondent mooring element is highlighted on the ship illustration located on the top right corner of each figure. As may be observed, the small passing distance associated to over speed pointed out in Figure 11 was responsible to strong interaction forces which led the moored ship to present large horizontal offsets and, consequently, high mooring loads. These results illustrate that the simulations based on simplified ship trajectories can be used as a first estimate of the operational limits for the passing ship problem in a specific berth, since they were confirmed when applying the ship paths obtained in the real-time simulations. On the other hand, it is clear that they are not sufficient for a full comprehension of the problem, since they do not guarantee that the ship can be maneuvered under the limits established which could only be evaluated by conducting real-time simulations commanded by experienced local pilots.

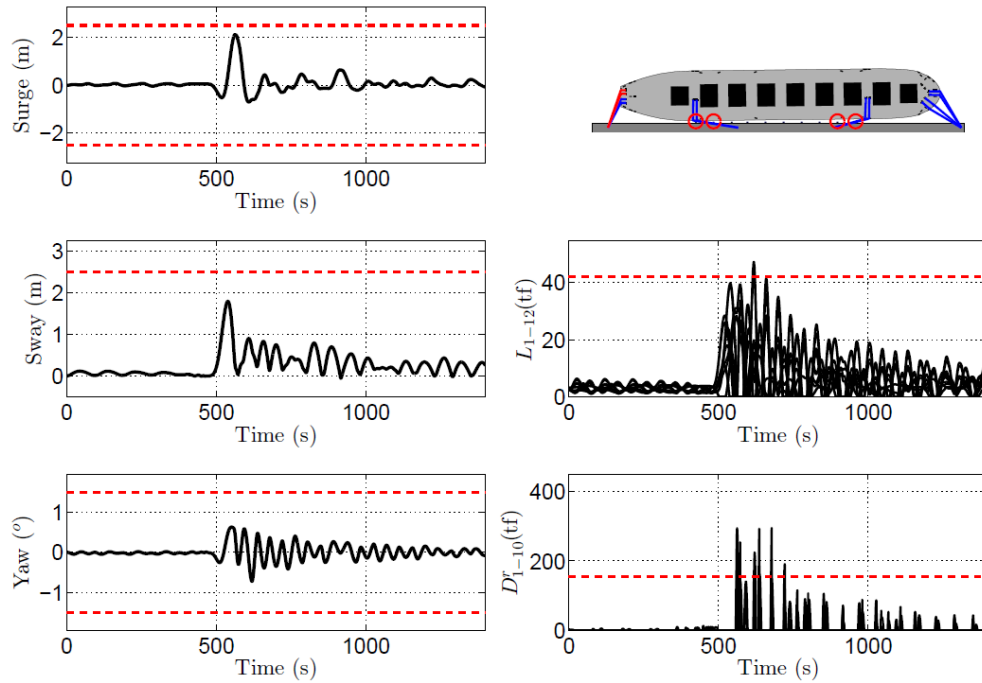


Figure 12: Case 4: Time histories of ship motions, mooring line loads and fender compression forces. Horizontal traced lines indicate tolerated margins

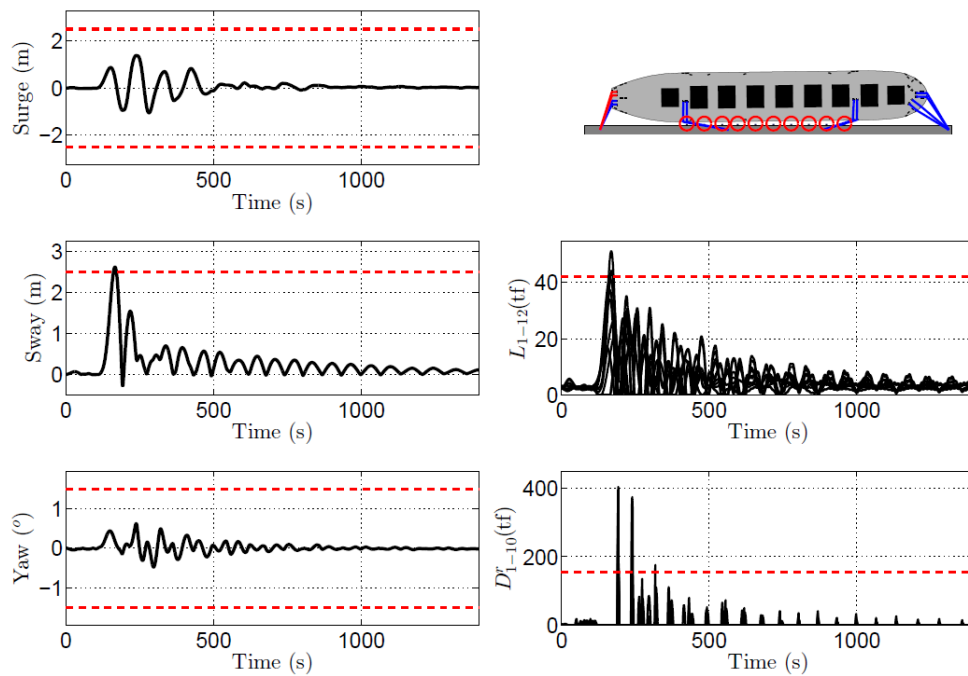


Figure 13: Case 6: Time histories of ship motions, mooring line loads and fender compression forces. Horizontal traced lines indicate tolerated margins

3.5. Improvements on the Mooring System

Two possibilities of improvements on the mooring system have been considered as an attempt to improve the mooring system performance observed in the cases 4 and 6. In the first, the two cases were tested assuming the same mooring arrangement, but increasing the lines pre-tensions to 6.6 tf (reasonable value to be applied in reality). The results are presented in Figure 14 and Figure 15 showing that the ship motions, lines loads and fenders compression forces become smaller by increasing the lines pre-tensions. In case 4, for example, this change was enough to reduce line loads to acceptable values. Nevertheless, it was not sufficient to reduce the sway amplitude and avoid the strong impacts between the ship and the fenders, which caused loads over 200tf in case 4 and 400tf in case 6.

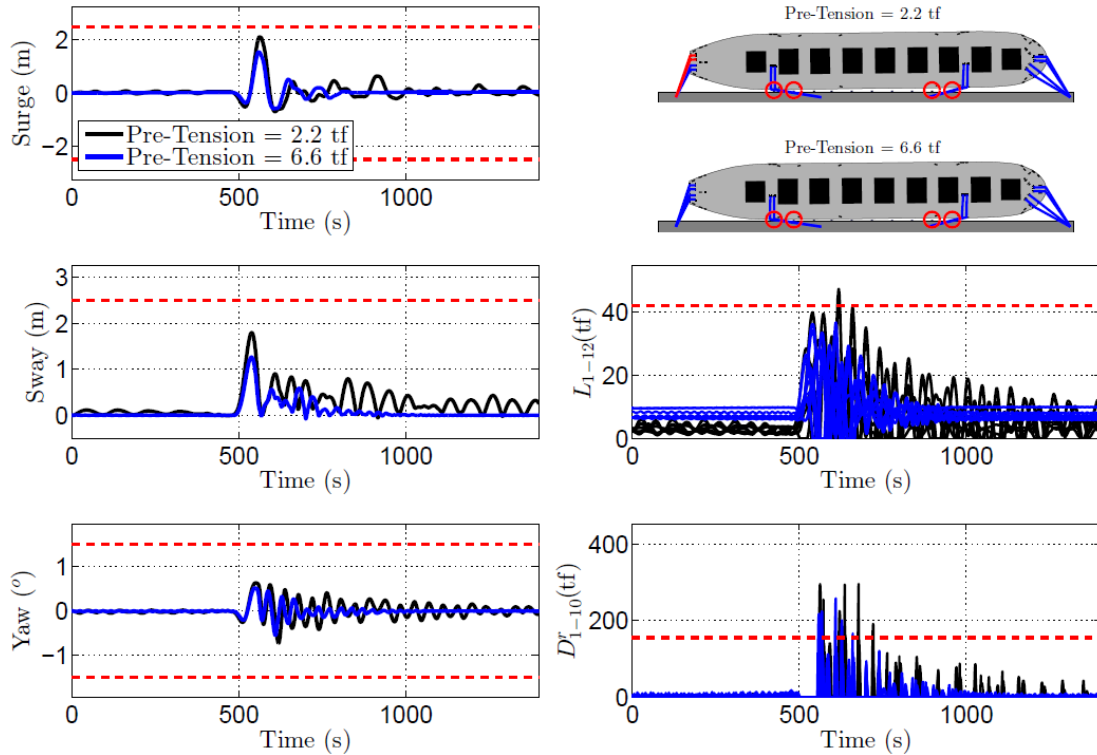


Figure 14: Case 4: Time histories of ship motions, mooring line loads and fender compression forces for two values of pre-tension. Horizontal traced lines indicate tolerated margins

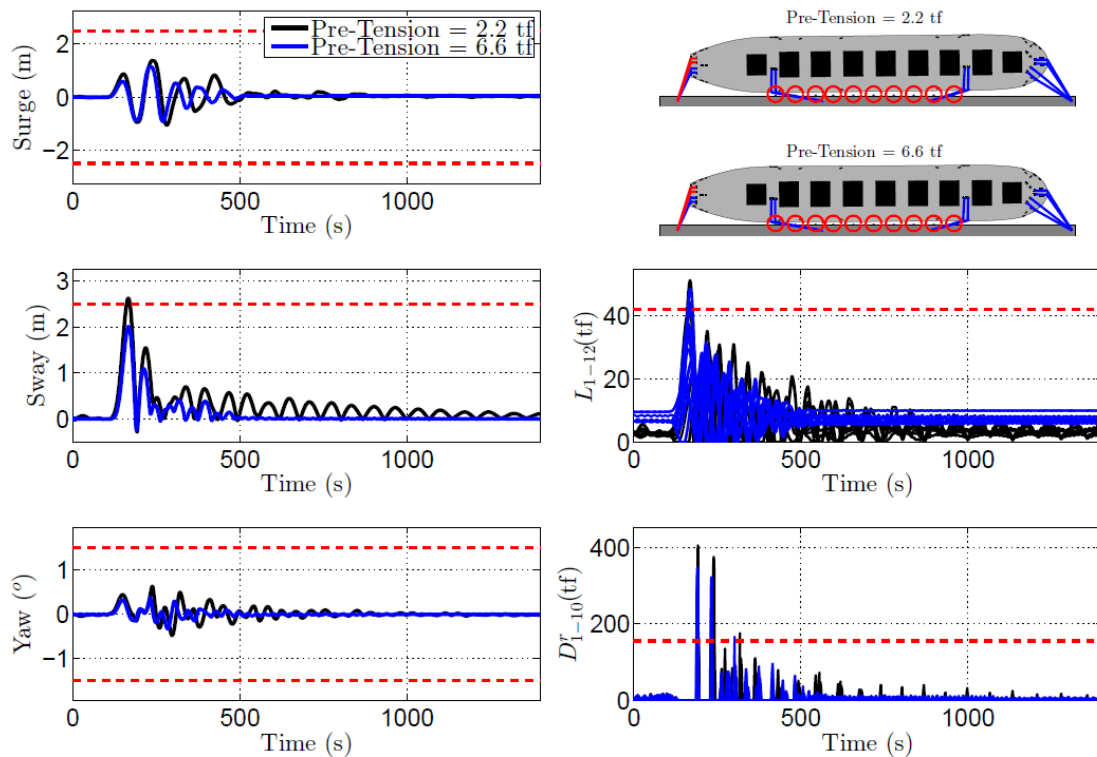


Figure 15: Case 6: Time histories of ship motions, mooring line loads and fender compression forces for two values of pre-tension. Horizontal traced lines indicate tolerated margins

The second test was performed by changing 2 stern lines and 2 head lines for stern and bow breast lines, as illustrated in Figure 16, increasing, therefore, the transversal and rotational stiffness of the mooring system. The results obtained are presented in Figure 17 and Figure 18 where reductions of the maximum sway and yaw motion amplitudes as well as the maximum mooring loads are observed. In case 6, however, practically all the fenders still exceeded the limit value, indicating that in this case a modification on the mooring system only would not be enough to avoid a problem, in which a change of the fenders to ones of more capacity would be indicated.

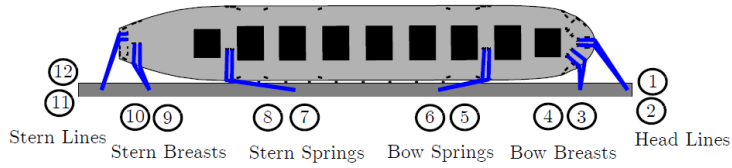


Figure 16: Alternative mooring arrangement of the small capsizes at berth 21

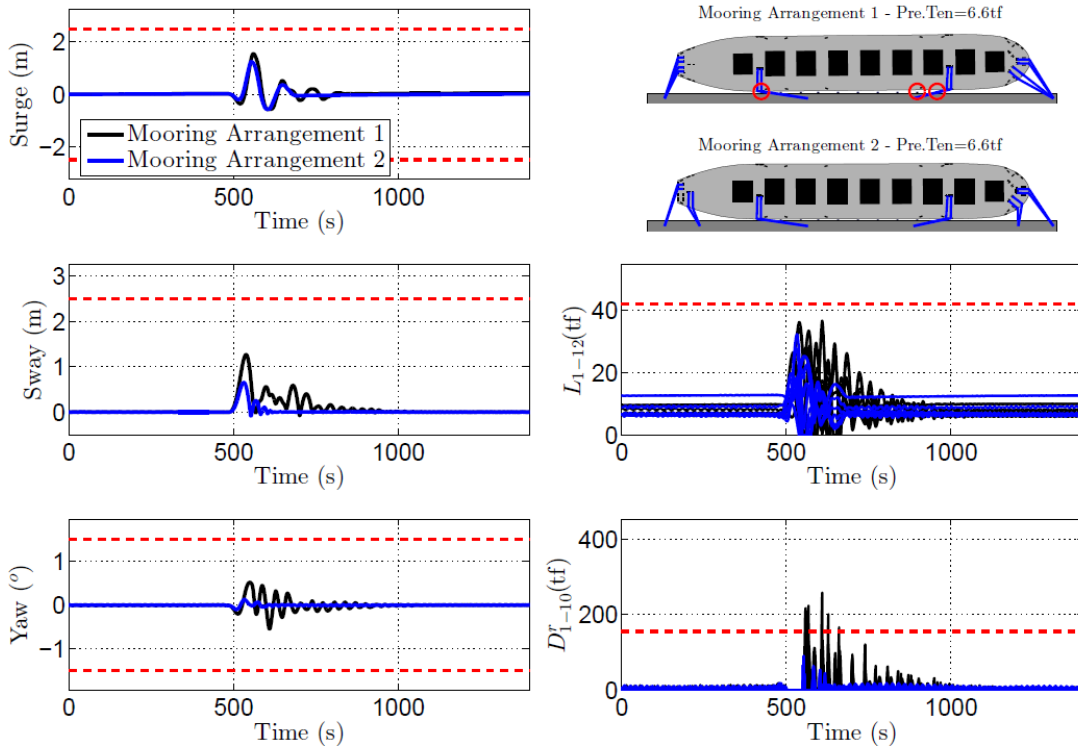


Figure 17: Case 4: Time histories of ship motions, mooring line loads and fender compression forces for two values of pre-tension. Horizontal traced lines indicate tolerated margins

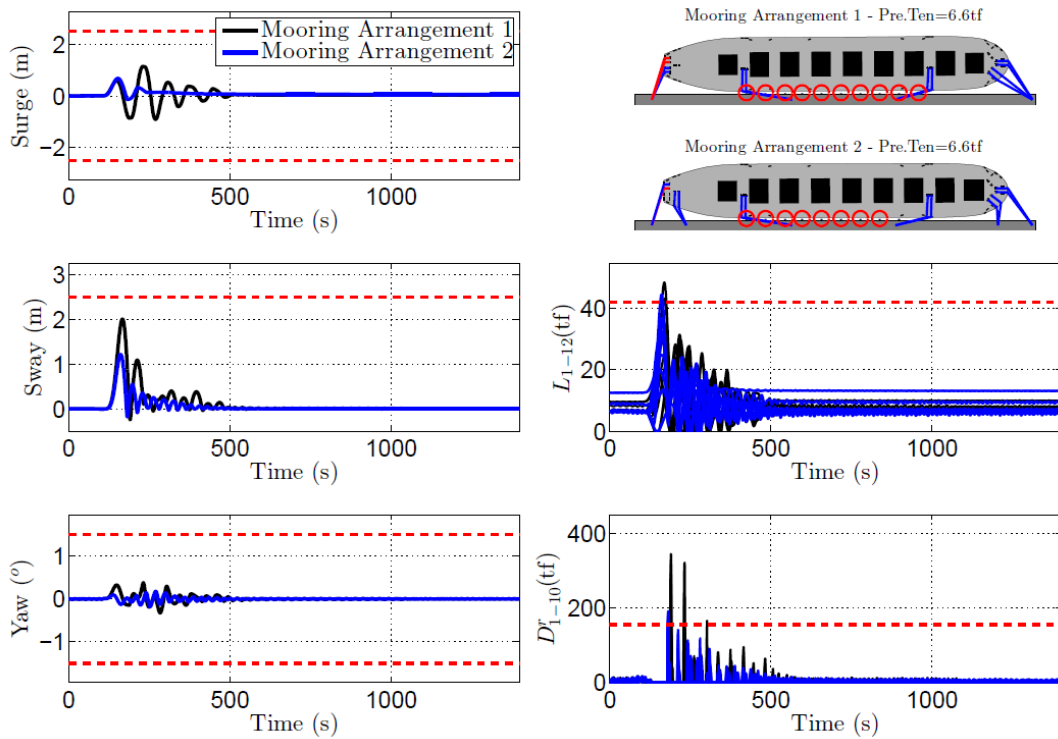


Figure 18: Case 6: Time histories of ship motions, mooring line loads and fender compression forces for two values of pre-tension. Horizontal traced lines indicate tolerated margins

4. CONCLUSIONS

An analysis methodology integrating a potential flow model, a dynamic simulator for moored ships and a real-time simulator was here presented for the assessment of the passing ship hydrodynamic problem.

From the results, it can be concluded that the standard approach of defining operational limits based on simplified ship trajectories can indeed be used as first estimate of the passing ship effect in a berth of interest, but requires special attention to the fact that they do not guarantee whether the ship can be maneuvered under the limits established. Therefore, it is indicated the conduction of real-time simulations commanded by experienced local pilots for a better understanding of the navigation scenario.

Besides the ship maneuvering aspect, the results have shown that significant improvements are obtained by setting the mooring lines with appropriate pre-tension values and also by choosing a mooring arrangement with higher transversal and rotational (in Z axis) stiffness, introducing, for instance, breast lines to the system. These measures tend to increase the mooring system safety, especially in situations where the pilot has to increase the ship speed so as to raise the rudder efficiency, what inevitably exposes the moored ships to higher passing ship forces.

5. ACKNOWLEDGMENTS

The authors gratefully acknowledge CODESP (Port Authority of Santos), represented by the company's president Jose Alex Botêlho de Oliva, for sponsoring this study. The authors also thank the Santos Pilots for their valuable advices and practical experience. Third author thanks the National Council for Scientific and Technological Development (CNPq process 308645/2013-8) for the research grant.

6. REFERENCES

- Cummins, W. (1962). The impulsive response function and ship motions. *Technical Report, Department of Navy David Taylor Model Basin.*
- Flory, J. (2002). The effects of passing ships on moored ships. *Prevention First 2002 Symposium, California State Lands Commission.*
- Hess, J., & Smith, A. (1967). Calculation of potential flow about arbitrary bodies. *Progress in Aerospace Sciences.*
- King, G. (1977). Unsteady hydrodynamic interactions between ships. *Journal of Ship Research.*
- Korsmeyer, F. T., Lee, C.-H., & Newman, J. N. (1993). Computation of ship interaction forces in restricted waters. *Journal of Ship Research.*
- Kriebel, D. (2005). Mooring Loads due to Parallel Passing Ships (Technical Report TR-6056-OCN). *Tech. rep., Naval Facilities Engineering Service Center.*
- Krishnankutty, P., & Varyani, K. (2004). Force on the Mooring Lines of a Ship due to the Hydrodynamic Interaction Effects of a Passing Ship. *International Shipbuilding Progress.*
- Muga, B., & Feng, S. (1975). Passing ship effects - from theory and experiment. *Offshore Technology Conference.*
- OCIMF. (2008). *Mooring Equipment Guidelines (MEG3), 3rd Edition.*
- Oortmerssen, G. (1976). The Motions of a Moored Ship in Waves. *Publication No 510 of the Netherlands Ship Model Basin, Wageningen, The Netherlands.*
- PIANC. (1995). *Criteria for Movements of Moored Ships in Harbours.* Rapport du Groupe de Travail n.27, Brussels (Belgium).
- Pinkster, J. (2004). The influence of a free surface on passing ship effects. *International Shipbuilding Progress.*
- Pinkster, J. A. (2009). Suction, Seiche and Wash Effects of Passing Ships in Ports. *SNAME Annual Meeting and Expo and Ship Production Symposium, Providence, Rhode Island, USA.*

PIANC-World Congress Panama City, Panama 2018

- Pinkster, J. A. (2014). A Fast, User-Friendly, 3-D Potential Flow Program for the Prediction of Passing Vessel Forces. *PIANC World Congress San Francisco, USA*.
- Remery, G. (1974). Mooring forces induced by passing ships. *Offshore Technology Conference*.
- Ruggeri, F., Watai, R., & Tannuri, E. (2016). Passing ships interactions in the oil terminal of São Sebastião (Brazil): An applied study to define the operation limits. *4th International Conference on Ship Manoeuvring in Shallow and Confined Water with Special Focus on Ship Bottom Interaction, May 23-25, Hamburg, Germany*.
- Talstra, H., & Blik, A. J. (2014). Loads on Moored Ships due to Passing Ships in a Straight Harbour Channel. *PIANC World Congress San Francisco, USA*.
- Tannuri, E., Rateiro, F., Fucatu, C., Ferreira, M., Masetti, I., & Nishimoto, K. (2014). Modular mathematical model for a low-speed maneuvering simulator. *Proceedings of the ASME 2014 33rd International Conference on Offshore Mechanics and Arctic Engineering OMAE2014*.
- Trelleborg. (2017). Trelleborg Marine Systems, Fender Systems Product Brochure.
- van der Hout, A., & de Jong, M. (2014). Passing Ship Effects in Complex Geometries and Currents. *PIANC World Congress San Francisco, USA*.
- Vantorre, M., Verzhbitskaya, E., & Laforce, E. (2002). Model test based formulation of ship-ship-interaction forces. *Ship Technology Research*.
- Wang, S. (1975). Dynamic Effects of Ship Passage on Moored Vessels. *ASCE Ports Proceedings, California, USA*.
- Watai, R. (2015). A Time Domain Boundary Elements Method for the Seakeeping Analysis of Offshore Systems. *PhD Thesis, University of São Paulo*.
- Watai, R., Ruggeri, F., Sampaio, C., & Simos, A. (2015). Development of a time domain boundary elements method for numerical analysis of floating bodies responses in waves. *Journal of the Brazilian Society of Mechanical Sciences and Engineering*.
- Watai, R., Ruggeri, F., Tannuri, E., & Weiss, J. (2013). Evaluation of empirical and numerical methods on the prediction of hydrodynamic loads involved in the passing ship problem. *3rd International Conference on Ship Manoeuvring in Shallow and Confined Water, June 3-5, Ghent, Belgium*.
- Wictor, E., & van den Boom, H. (2014). Full Scale Measurements of Passing Ship Effects. *PIANC World Congress San Francisco, USA*.